Numerical modelling study on the flexural uplift of the Transantarctic Mountains

Tadashi Yamasaki, [1,2] Hideki Miura[3] and Yoshifumi Nogi[3]

[1]*Dublin Institute for Advanced Studies, 5 Merrion Square, Dublin* 2, *Ireland*
[2]*Department of Tectonics, Faculty of Earth and Life Sciences, VU University Amsterdam, De Boelelaan* 1085, 1081 *HV Amsterdam, the Netherlands.*
E-mail: tadashi.yamasaki@falw.vu.nl
[3]*National Institute of Polar Research,* 1-9-10 *Kaga, Itabashi-ku,* 173-8515 *Tokyo, Japan*

SUMMARY

In this study, based on a 2-D thermomechanical finite element model, the uplift of the Transantarctic Mountains (TAM) is discussed in relation to the flexural uplift of a rheologically layered lithosphere, which is described by Vening-Meinesz's cantilever kinematics. The general model behaviour shows that the thickness of the crust and the geothermal gradient in the lithosphere are the principal factors in controlling the effective elastic thickness (T_e). Although T_e is also significantly dependent on the magnitude of the uplift and the wet or dry rheological condition of rocks, these two factors do not have a dominant influence on the half-wavelength of the TAM. The model with a plausible crustal structure beneath Antarctica shows that the thermal structure beneath East Antarctica is the critical factor, controlling the half-wavelength of the TAM. If there is a significant radiogenic heat source in the Antarctic lithosphere, T_e beneath East Antarctica is estimated to be 50 km, at most, and the lithosphere has no potential to explain an exceptionally large-scale half-wavelength of the TAM. Even for the model without a heat source, if East Antarctica is significantly thermally influenced by West Antarctica, T_e is estimated to be about 60 km, and it is difficult to reproduce the half-wavelength of the TAM. Contrarily, when a radiogenic heat source is absent and the thermal structure beneath East Antarctica is not significantly affected by that beneath West Antarctica, the rheological structure beneath East Antarctica has the potential to reproduce the half-wavelength of the TAM ($T_e \sim 100$ km). Thus, the presence of a radiogenic heat source in the crust and mantle and the thermal influence of West Antarctica on East Antarctica are crucial factors in the reproduction of the half-wavelength found in the TAM.

Key words: Lithospheric flexure; Rheology: crust and lithosphere; Rheology: mantle; Antarctica.

GJI Tectonics and geodynamics

1 INTRODUCTION

Surface deflection cannot be understood without the concept of lithospheric strength. The strength of the lithosphere is characterized by the flexural rigidity D, given by the equation $D = [12 \, h(1 - \nu^2)/E]$, where h is the elastic thickness, ν is Poisson's ratio and E is Young modulus. To evaluate the lithospheric strength, h has been constrained by matching numerical prediction to observed surface topography. However, the deformation mechanisms derived from laboratory experiments that include not only elastic but also brittle and ductile deformation, should be taken into account in the stress distribution in the lithosphere (e.g. Sibson 1977; Goetze & Evans 1979; Kirby 1983; Carter & Tsenn 1987; Ranalli & Murphy 1987; Kohlstedt *et al.* 1995). Therefore, we have to know how the rheologically layered lithosphere would respond to an applied load to evaluate the effective elastic thickness (T_e), which is a measure of the effective strength of the total lithosphere (e.g. Burov & Diament 1992, 1995).

Rift flank uplift has been discussed in terms of the flexural response of the mechanical lithosphere (e.g. Artemjev & Artyushkov 1971; Braun & Beaumont 1989; Weissel & Karner 1989; Ebinger *et al.* 1991; Kooi *et al.* 1992; van der Beek *et al.* 1994; van der Beek 1997). Similarly, the flank uplift in the Ross Sea rift system, characterized by the prominent uplift of the Transantarctic Mountains (TAM, Fig. 1), also gives an excellent opportunity to study the strength of the lithosphere. The present elevation of the TAM is up to 4500 m (e.g. Robinson & Splettstoesser 1984), and its half-wavelength, defined by the distance from the maximum uplift to the deepest point, is of the order of 500 km (e.g. Stern & ten Brink 1989). This is exceptionally large-scale flank uplift in comparison with the typical height of 1000–2000 m and half-wavelength of 200–300 km observed in many other rift systems (e.g. Steckler 1985; Weissel & Karner 1989; van der Beek *et al.* 1994).

Several numerical studies have been carried out on the TAM. Simple elastic (Stern & ten Brink 1989; ten Brink & Stern 1992; ten Brink *et al.* 1997) and viscoelastic (Bott & Stern 1992) models

Figure 1. Location map of the Transantarctic Mountains (TAM) in Antarctica.

have shown that the most important parameter controlling the uplift of the TAM is the elastic thickness, in which the half-wavelength of the TAM essentially requires an elastic thickness of about 100 km (whereas a relatively thin elastic layer, 5–25 km, beneath the mountain front is required to obtain sufficient uplift). However, since the surface deflection should reflect the integrated effect of the various deformation mechanisms in the lithosphere (e.g. Burov & Diament 1995), it is important to investigate whether the half-wavelength of the TAM can be obtained by the flexural uplift of a rheologically layered lithosphere beneath East Antarctica.

In this study, the flexural uplift of the TAM, especially its half-wavelength, is discussed on the basis of a 2-D thermomechanical finite element model in which the viscoelastic–perfect plastic (VEP) rheology model is implemented, including temperature-dependent viscosity. Based on a model with uniform crustal and thermal structures, we examine the general model behaviour first to understand what primarily controls the half-wavelength of the flexural uplift. We then evaluate whether the rheological structure of the Antarctic lithosphere has the potential to produce the half-wavelength of the TAM, respecting the lithospheric structure beneath the Antarctica inferred from geophysical observations. The presence of the ice sheet in East Antarctica is also taken into account. This study shows that the presence of a radiogenic heat source in the crust and mantle and the thermal influence of West Antarctica on East Antarctica are the critical factors to reproduce the half-wavelength of the TAM.

2 GEOLOGICAL BACKGROUNDS AND LITHOSPHERE CONFIGURATION

The TAM is situated over a distance of about 3500 km along the morphological and geological boundary between East and West Antarctica (Fig. 1). Apatite fission track analysis revealed that the uplift of the TAM began about 50 Ma in the Cenozoic, and uplift of rocks during the last 50 Myr reaches up to 7000–8000 m (e.g. Fitzgerald *et al.* 1986; Fitzgerald 1992, 1994). Radio echo-sounding found a distinct basin (the Wilkes Basin) running parallel to the TAM in which the axis of the basin is about 500 km behind the mountain front (e.g. Drewry 1976, 1983). A negative free-air gravity anomaly of −20 to −60 mGal is observed over the Wilkes Basin, which ranges from the North Victoria Land nearly to the South Pole, with the anomaly minimum at the deepest point of the basin (e.g, Drewry 1976; Bentley 1983; Stern & ten Brink 1989). Drewry

(1976), Bentley (1983) and Steed (1983) explained the origin of the gravity anomaly in terms of the upper crustal sediments with a thickness of 2–3 km. However, Stern & ten Brink (1989) objected to this interpretation, proposing the lithospheric flexure model as the origin of the gravity anomaly. This is because the large-scale sediment load must be compensated, and it is difficult to explain the gravity anomaly. Based on the flexure model, Stern & ten Brink (1989) defined the distance from the mountain front to the axis of the basin as the half-wavelength of the TAM's uplift (∼500 km). It is also noted that the surface deflection in the Ross Sea region seems to have a half-wavelength of 160–230 km (Stern & ten Brink 1989).

Cooper *et al.* (1991a, b) indicated that the Ross Sea rift system was developed by at least two distinct rifting events, and the uplift of the TAM has occurred along with the later rifting event. The earlier rifting event that occurred in the late Mesozoic, seems to cause the crustal thinning over a widespread region in West Antarctica. However, the later rifting event in the Cenozoic concentrated mainly along the TAM, the Terror rift and the Marie Byrd Land. ten Brink *et al.* (1993) indicated that the earlier rifting event in West Antarctica preceded the onset of the TAM's uplift by at least 20 Myr.

The lithospheric structure beneath Antarctica can be inferred from geophysical observations. The crustal structure beneath East and West Antarctica has been constructed by seismic reflection and refraction studies (e.g. ten Brink *et al.* 1993; Bannister *et al.* 2003; Lawrence *et al.* 2006) from which the crustal thickness beneath East Antarctica is 35–40 km and that beneath West Antarctica is about 20 km.

Seismic tomography beneath Antarctica (Sieminski *et al.* 2003) implies that the thicknesses of the lithosphere beneath East and West Antarctica are likely to be between 200 and 300 km and less than 100 km, respectively. Thus, the thickness of the lithosphere seems enormous beneath East Antarctica but much thinner beneath West Antarctica, which is also seen in the surface wave studies of Danesi & Morelli (2000, 2001). The observed surface heat flow in the Ross Sea is consistent with such hot lithosphere beneath West Antarctica (e.g. Blackman *et al.* 1987; Berg *et al.* 1989; Della Vedova *et al.* 1992). The thermal structure beneath West Antarctica seems to be attributable to the earlier rifting event, not to the later rifting event (e.g. Cooper *et al.* 1991a, b).

The ice sheet in East Antarctica appeared at about 36 Ma (e.g. Barrett *et al.* 1989; Zachos *et al.* 1989; Barker *et al.* 1999; Zachos *et al.* 2001) as clearly implied by the record of the oxygen isotope (e.g. Miller *et al.* 1987). From then on, the ice sheet fluctuated frequently. However, during the last 14 Myr, the ice sheet has mostly maintained the same size as at present, with its maximum size attained around 11 Ma (Woodruff *et al.* 1981).

3 DESCRIPTION OF THE NUMERICAL MODEL

The Vening-Meinesz flexural cantilever model (Vening-Meinesz 1950) is most likely to be appropriate for the uplift of the TAM, as adopted in prior studies (Stern & ten Brink 1989; Bott & Stern 1992; ten Brink & Stern 1992; ten Brink *et al.* 1997). There is no uplift on the other side of the Ross Sea rift, and the geomorphology is evidently asymmetric between East and West Antarctica. In addition, van der Beek *et al.* (1994) indicated that the necessary amount of the uplift requires a simple shear component just below the edge of the mountain range. Furthermore, seismic reflection and refraction studies have never detected a low-angle detachment fault (e.g. ten Brink *et al.* 1993; Bannister *et al.* 2003).

An alternative model of the TAM has been proposed by Bialas *et al.* (2007). They indicated that the TAM was a part of high-elevation plateau with a considerably thick crustal root prior to continental extension, and the present elevation of the mountain is only a remnant edge of the Ross Sea rift. In their numerical model, the initial Moho temperature is the critical factor to explain the observed extensional feature in the Ross Embayment. However, there is no evidence supporting the initial temperature at the Moho. Additionally, the difference in lithosphere thickness between East and West Antarctica (e.g. Sieminski *et al.* 2003) was not taken into account in their numerical experiments of continental extension. If significant thickness heterogeneity of the lithosphere is present, the deformation would focus on the transitional position between hot and cold lithospheres (Pascal *et al.* 2002), and the localized deformation may be responsible for the development of the lithosphere-cutting shear zone (e.g. Pascal *et al.* 2004). Similarly, numerical (Huerta & Harry 2007) and analogue (Bonini *et al.* 2007) models showed that the extensional deformation can be significantly localized into the transitional position between East and West Antarctica. Therefore, it may be more reasonable to consider that the development of the TAM is associated with the movement of the border fault between East and West Antarctica.

Fig. 2 shows schematically, the 2-D thermomechanical model adopted in this study. We examine the response of the rheologically layered lithosphere to the applied horizontal constant boundary velocity (V_x) in Vening-Meinesz's cantilever kinematics. Mechanical and thermal problems are solved by using a finite element method. The plane strain condition is assumed for the 2-D model. We assume that the lithosphere has three compositional layers: quartzite upper crust, anorthite lower crust and dunite mantle.
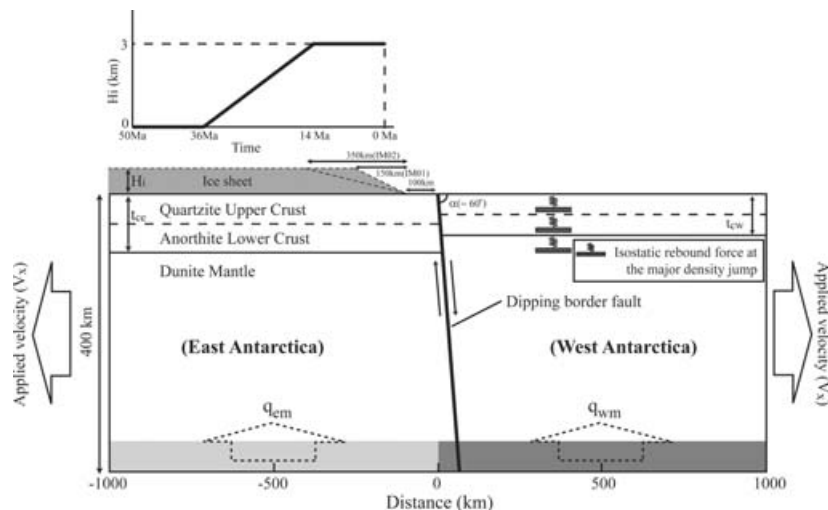
The model is divided into two domains by the border fault, and the left- and right-hand halves of the model are regarded as the East and West Antarctica, respectively. The crustal thicknesses beneath East (t_{ce}) and West (t_{cw}) Antarctica are 40 and 20 km, respectively. The thickness of the lower crust is half of the entire crust. The reduced heat flow beneath East Antarctica (q_{em}) is different from that beneath West Antarctica (q_{wm}) to obtain the heterogeneity of the lithosphere thickness. However, uniform lithospheric structure in the whole model is used to examine the general model behaviour in Section 4, where t_{ce} and t_{cw} are equal to t_c and the reduced heat flow q ($= q_{em} = q_{wm}$) is applied to obtain uniform thickness of the thermal lithosphere (a).

3.1 The rheological model

Under low deviatoric stress conditions, isotropic linear elastic behaviour is a good approximation of rock deformation, in which the strain is linearly related to the stress by the generalized Hooke's law (e.g. Ranalli 1995). However, under larger deviatoric stresses, different deformation mechanisms become more important.

Under low temperature and pressure conditions, deformation of rocks takes place in a brittle manner. The stress-level (σ_b) required for frictional sliding on the fault is given by the Byerlee's law (Byerlee 1967, 1978). In this study, we simply express Byerlee's law in an approximate form

$$\sigma_b = \zeta(1 - \upsilon^*)z, \tag{1}$$

where ζ is the constant (24 MPa km^{-1}), υ^* is the density ratio of pore water to rock matrix ($\upsilon^* = 0.4$ for wet rheology and $\upsilon^* = 0$

Figure 2. Schematic figure of the numerical model adopted in this study. The model is divided into two domains by the border fault, with the left- and right-hand halves of the model being regarded as East and West Antarctica, respectively. The lithosphere has three compositional layers: quartzite upper crust, anothite lower crust and dunite mantle. The thickness of the crust beneath East and West Antarctica is t_{ce} and t_{cw}, respectively. A horizontal boundary velocity V_x is applied at the right- and left-hand ends of the model. The Winkler restoring force is applied at the surface, the boundary between upper and lower crust, and the Moho to calculate the vertical surface movements. The border fault that penetrates to the bottom of the model is incorporated by means of the slippery node method (Melosh & Williams 1989). The dip-angle, α, of the fault is assumed to be 60°. The thermal boundary condition of the model is as follows. The horizontal heat flow is zero at the right- and left-hand side boundaries of the model. The temperature of the surface is fixed to be 0 °C. The reduced heat flow q_{em} and q_{wm} is applied beneath the East and West Antarctica, respectively, satisfying the condition that the temperature at the base of a given thermal lithosphere beneath East and West Antarctica is equal to the potential temperature of the asthenosphere (1350 °C). At the depth below the thermal lithosphere, the temperature is imposed to be the potential temperature of the asthenosphere. Note that uniform lithospheric structure in the whole model—$t_c = t_{ce} = t_{cw}$ and $q = q_{em} = q_{wm}$— is used to examine the general model behaviour. In the application to the TAM, the external load of the ice sheet is introduced in terms of the pressure vertically operating on the surface in the East Antarctica. Two ice sheet models are adopted in this study: IM01 and IM02. The thickness of the ice sheet is H_i at most. It is assumed that H_i linearly increases from 0 to 3 km with time over the periods between 36 and 14 Ma and is constant from then on. The density of the ice is assumed to be 900 kg/m^3.

for dry rheology) and z is the depth in km (e.g. Brace & Kohlstedt 1980; Ranalli 1995).

We adopt the elastic–perfect plastic rheology for the brittle deformation (e.g. Fletcher & Hallet 1983; Braun & Beaumont 1987; Braun 1988; Bassi 1991, 1995) in which the state of the stress is controlled by the Von Mises yield criterion F:

$$F = J_{2D} - \frac{1}{3}\sigma_y^2 = 0, \tag{2}$$

where σ_y is the yield stress and J_{2D} is the second invariant of deviatoric stress. Once the state of the stress exceeds the failure criterion, an instantaneous material flow occurs according to the perfect plastic flow law. The yield stress σ_y is equivalent to σ_b in eq. (1), so that σ_y is a function of the depth z.

On the other hand, under high temperature and pressure conditions, rocks deform in a ductile manner. In this study, the non-linear Maxwell viscoelastic rheology is adopted for the ductile behaviour of rocks (e.g. Braun & Beaumont 1987; Govers & Wortel 1993, 1995). It is assumed that the viscous flow is controlled by the power-law creep (e.g. Kirby 1983; Carter & Tsenn 1987), where the effective viscosity η can be written in a form

$$\eta = \frac{1}{2A^*} J_{2D}^{\frac{1-n}{2}} \exp\left(\frac{Q}{R\Theta}\right), \tag{3}$$

where A^* is a material constant, Q is the activation energy, n is the stress exponent, R is the universal gas constant and Θ is the absolute temperature. In the calculations A^* is multiplied by a factor of $3^{(n+1)/2}/2$ (Ranalli 1995). Flow law parameters of each rock composition are shown in Table 1.

3.2 The mechanical model

The finite element code, tekton ver.2.1 (Melosh & Raefsky 1980, 1981; Melosh & Williams 1989), is used to solve the mechanical equilibrium equation

$$\nabla \cdot \sigma + \mathbf{X} = 0, \tag{4}$$

where σ is the stress tensor and $\mathbf{X}$ is the body force. The constant extensional velocity (V_x) is adjusted to obtain the magnitude of the uplift at the mountain front (ξ) during the extensional period of ΔD_t. The non-linear Maxwell viscoelastic behaviour can be solved by the original version of the code.

We have modified the tekton code to solve the VEP rheology problem with temperature-dependent viscosity. The effective viscosity as a function of temperature and stress is implemented into the code, according to eq. (3). Additionally, following Krieg & Krieg (1977), Braun & Beaumont (1987) and Braun (1988), the stress in

Table 1. Model parameter values used in this study.

Symbol	Meaning	Value
E	Young's modulus	1.5×10^{11} Pa
ν	Poisson's ratio	0.25
ζ	Depth dependence of brittle failure	24.0 MPa km^{-1}
υ^*	Density ratio of pore water to rock	0.4
C_p	Specific heat	1050 Jkg^{-1} K^{-1}
T_a	Asthenospheric potential temperature	1350 °C
ρ_{uc}	Mass density of the upper crust	2800 kg m^{-3}
ρ_{lc}	Mass density of the lower crust	2900 kg m^{-3}
ρ_m	Mass density of the mantle	3300 kg m^{-3}
H_{uc}	Heat production in the upper crust	1.37 μW m^{-3}
H_{lc}	Heat production in the lower crust	0.45 μW m^{-3}
H_m	Heat production in the mantle	0.02 μW m^{-3}
K_{uc}	Thermal conductivity of the upper crust	2.56 W m^{-1} K^{-1}
K_{lc}	Thermal conductivity of the lower crust	2.60 W m^{-1} K^{-1}
K_m	Thermal conductivity of the mantle	3.20 W m^{-1} K^{-1}
Flow law parameters of power-law creep		
Wet Quartzite: Koch et al. (1989)		
$A*_{ucw}$	Pre-exponent	1.10000×10^{-21} Pa^{-n} s^{-1}
n_{ucw}	Power	2.61
Q_{ucw}	Activation energy	145 kJmol^{-1}
Dry Quartzite: K och et al. (1989)		
$A*_{ucw}$	Pre-exponent	5.58000×10^{-24} Pa^{-n} s^{-1}
n_{ucw}	Power	2.72
Q_{ucw}	Activation energy	134 kJmol^{-1}
Anorthite: Shelton & Tullis (1981)		
$A*_{lc}$	Pre-exponent	5.60000×10^{-23} Pa^{-n} s^{-1}
n_{lc}	Power	3.20
Q_{lc}	Activation energy	238 kJmol^{-1}
Wet Aheim Dunite: Chopra & Paterson (1984)		
$A*_{mw}$	Pre-exponent	5.4954×10^{-25} Pa^{-n} s^{-1}
n_{mw}	Power	4.48
Q_{mw}	Activation energy	498 kJmol^{-1}
Dry Aheim Dunite: Chopra & Paterson (1984)		
$A*_{md}$	Pre-exponent	7.24436×10^{-18} Pa^{-n} s^{-1}
n_{md}	Power	3.60
Q_{md}	Activation energy	535 kJmol^{-1}

the VEP rheology is computed by using the radial return algorithm. In each time step, the viscoelastic stress within the each element of the model is calculated as the trial stress σ^{tr} to check whether or not brittle failure occurs. When the trial stress exceeds the failure criterion [$F(\sigma^{tr}) > 0$], brittle deformation occurs and the true stress σ is computed by projecting the trial stress normally on the failure envelope (e.g. Krieg & Krieg 1977; Braun & Beaumont 1987; Braun 1988):

$$\sigma = \sqrt{\frac{\sigma_b^2}{J_{2D}^{tr}}}\sigma'^{tr} + \mathbf{P}^{tr} \qquad (5)$$

where σ'^{tr} is the trial deviatoric stress, J_{2D}^{tr} is the second invariant of the trial deviatoric stress and $\mathbf{P}^{tr}$ is the trial pressure. Contrarily, when the trial stress does not exceed the failure criterion [$F(\sigma^{tr}) < 0$], deformation is viscoelastic and the trial stress can, therefore, be regarded as the true stress.

The isostatic rebound force at the interface of a density jump is simulated using the Winkler restoring force (e.g. Melosh, unpublished; Williams & Richardson 1991). In this study, the Winkler restoring force is set at the following interfaces of major density jumps: the surface, the boundary between the upper and lower crust and the Moho (see Fig. 2). Although the density of rocks is a function of temperature, the density contrast at the each interface is simply evaluated at a temperature of 0 °C.

In the flexural cantilever model, deformation of the lithosphere is principally controlled by the sliding along the border fault. The movement of the fault is simulated using the slippery node method that has been incorporated into the original version of the code (Melosh & Williams 1989). We ignore the frictional resistance on the fault, so that the sliding takes place to keep the shear stress on the fault at zero.

The geometry of the border fault adopted in this study is similar to that in Bott & Stern (1992). The dipping border fault penetrates to the bottom of the model, and the constant dip-angle α is 60° (see Fig. 2). We have confirmed that the extent depth of the border fault does not change the model results significantly as long as the fault penetrates through the mechanically competent layer that deforms in elastic manner. If the lithosphere is strong enough to have the competent layer, the fault may possibly penetrate the crust and mantle lithosphere (Huismans & Beaumont 2002). The TAM border fault may also cut the whole lithosphere because the extreme lateral variation in lithospheric thickness inferred beneath East and West Antarctica focuses deformation, producing a large-scale shear zone (e.g. Petit & Ebinger 2000; Pascal *et al.* 2002; Pascal *et al.* 2004; Bonini *et al.* 2007; Huerta & Harry 2007).

Uplift of the surface is defined by uplift of rocks and exhumation; uplift of rocks and exhumation are referred to as displacements of rocks with respect to the geoid and the surface, respectively (England & Molnar 1990). Uplift of rocks would include both tectonic uplift and isostatic rebound effect associated with exhumation. Even though it is difficult to assume the absence of exhumation, we dare to ignore its effect. Our main purpose is to investigate the half-wavelength of the TAM's uplift. The half-wavelength of the mountain will not be affected significantly by the isostatic response to exhumation because the lateral space scale of exhumation must be less than the half-wavelength of the uplift. Even in the prior studies, which included the effect of exhumation and sediment loading in the hinterland, the most important factor controlling the half-wavelength of the TAM was still the elastic thickness (Stern & ten Brink 1989; Bott & Stern 1992; ten Brink & Stern 1992; ten Brink *et al.* 1997). In this study, the force driving the uplift of

the mountain is imposed only to the applied boundary velocity, and the half-wavelength for a given magnitude of uplift is discussed in relation to the lithospheric rheology.

3.3 The thermal model

Since power-law creep is a thermally activated process, the mechanical model should be coupled with the thermal model. In this study, we have developed a finite element code to solve the steady-state heat equation

$$\nabla \cdot (\mathbf{K}\nabla T) + H = 0, \qquad (6)$$

where T is the temperature, $\mathbf{K}$ is the thermal conductivity tensor and H is the radiogenic heat source. Parameter values used in this study are shown in Table 1. The same finite element grid as that for the mechanical model, is used for solving the thermal model. Thermal boundary conditions of the model are as follows. At the left- and right-hand side boundaries of the model, the horizontal heat flow is zero. The temperature at the surface is held at 0 °C. The potential temperature of the asthenosphere (T_a) is assumed to be 1350 °C. The reduced heat flow is applied to satisfy that the temperature at the base of a given thermal lithosphere is equal to T_a, which means that the thickness of the thermal lithosphere is defined by the 1350 °C isotherms. The temperature below a given thermal lithosphere is imposed to be T_a. The solution of eq. (6) is adopted as the initial condition. The temporal change in temperature is not evaluated in this study because the predicted deformation of the lithosphere is too small to produce any significant thermal perturbations.

In this study, we construct two models of the thermal structure beneath Antarctica: TM01 and TM02. Based on the study of seismic tomography in Antarctica (Sieminski *et al.* 2003), we assume that the maximum thickness of thermal lithosphere beneath East Antarctica (a_e) is 250 km and that beneath West Antarctica (a_w) is 90 km. In the TM01 model, the reduced heat flows of q_{em} and q_{wm} are adjusted to satisfy that the temperatures at depths of 250 and 90 km on the left- and right-hand boundaries of the model, respectively, are equal to T_a. In the TM02 model, the temperature profiles for the uniform model with $t_c = 40$ km and $a = 250$ km and for the model with $t_c = 20$ km and $a = 90$ km are artificially adopted in East and West Antarctica, respectively.

3.4 The ice sheet model

The load of the ice sheet is introduced in terms of a pressure, operating vertically on the upper surface of the model at a distance between −1500 and −100 km. The density of the ice is assumed to be 900 kg m^{-3}. In this study we use two models, IM01 and IM02, for the distribution of the ice sheet. The thickness of the ice sheet is H_i, at most, and linearly decreases to zero over the distance from −250 to −100 km and from −450 to −100 km for the IM01 and IM02 models, respectively (see Fig. 2). H_i is 3 km at the present time (e.g. Stern & ten Brink 1989). H_i increased linearly between 36 and 14 Ma and has stayed constant from 14 Ma to the present (see also Fig. 2). It is noted that the IM01 model is identical to that adopted in ten Brink *et al.* (1997).

4 MODEL RESULTS

4.1 General model behaviour of the VEP model

Although our main purpose is to investigate the uplift of the TAM, it is necessary to understand what primarily controls the flexural uplift of the rheologically layered lithosphere, beforehand. Therefore, in
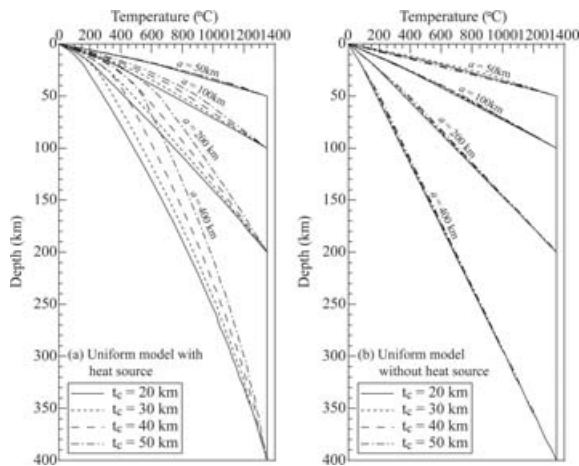
Figure 3. Temperature distribution in the lithosphere for different t_c and a for the uniform model; (a) model with radiogenic heat source and (b) model without radiogenic heat source.

this subsection, we briefly describe the general model behaviour of the VEP model with the uniform lithospheric structure, though the essential points have already been reported in earlier studies (e.g. Burov & Diament 1995).

4.1.1 The modelled temperature distribution in the lithosphere

We first show the temperature distribution in the lithosphere for the models with and without a radiogenic heat source in the crust and mantle (see Fig. 3). The smaller geothermal gradient can be clearly seen in the model with a greater thickness of thermal lithosphere (a). The geothermal gradient is also smaller in the model without a heat source than in the model with a heat source. These imply that the predicted surface deformation would be significantly influenced by a and the presence of a heat source.

In the model with a heat source, the thickness of the crust (t_c) is also an important factor in controlling the temperature distribution in the lithosphere, but its importance is weaker for smaller a. No significant difference in the temperature distribution, brought about by the difference in t_c, can be seen for the model with $a = 50$ km. In contrast, in the model without a heat source, the temperature distribution in the lithosphere is mostly insensitive to t_c, which implies that the dependence of the surface deformation on t_c would be related to the difference in rock composition between the crust and mantle.

4.1.2 The surface deflection in the VEP model with uniform lithosphere structure

Fig. 4 shows the surface deformation predicted by the VEP model with a heat source. The wet rheology condition is adopted for the model here. The extensional velocity (V_x) is adjusted to obtain the magnitude of the uplift at the mountain front $\xi = 5$ km at time $t = 50$ Myr. The general model behaviour is as implied from the thermal structure of the lithosphere, shown in Fig. 3. For the model with $a = 50$ km, the surface deformation is mostly insensitive to t_c. On the other hand, in the model with $a \geq 100$ km, it can be seen that the surface deformation is significantly dependent on t_c.

Fig. 5 shows the surface deformation predicted by the VEP model without a heat source. The wet rheology condition is also adopted for this model. Significant dependence on t_c appears in the model with $a = 100$ and 200 km, even though any difference in the geothermal gradient cannot be seen for different t_c (see Fig. 3b). This is because the crust is intrinsically weaker than the mantle without any thermal effects. On the other hand, the surface deformation is mostly insensitive to t_c for the model with $a = 50$ or 400 km, because the geothermal gradient is too high or too low for any significant difference in rheological property between the lower crust and mantle to be perceptible.
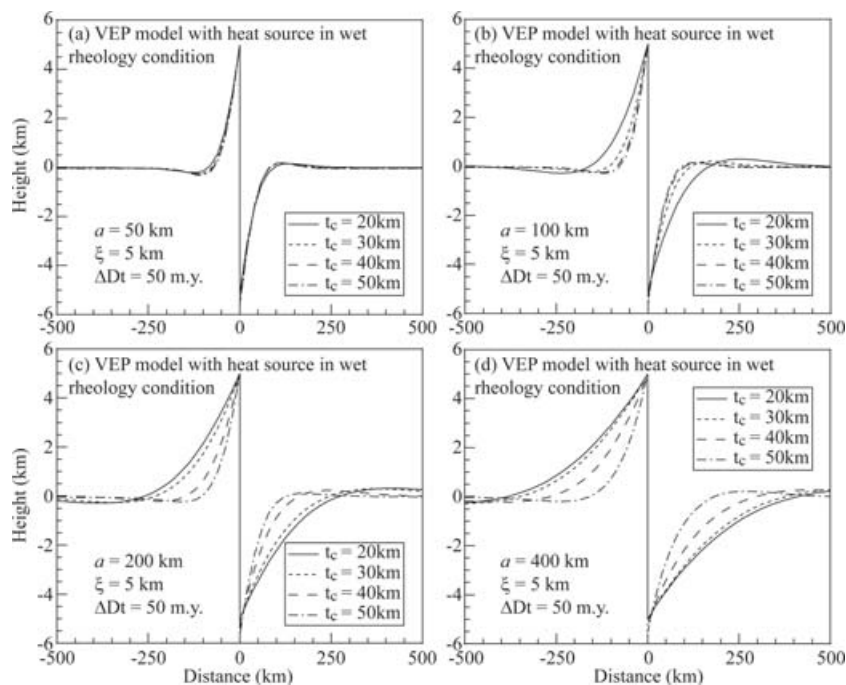

Figure 4. Surface deformation predicted by the viscoelastic–perfect plastic (VEP) model with heat source in wet rheology condition for different t_c; (a) $a = 50$ km, (b) $a = 100$ km, (c) $a = 200$ km and (d) $a = 400$ km.
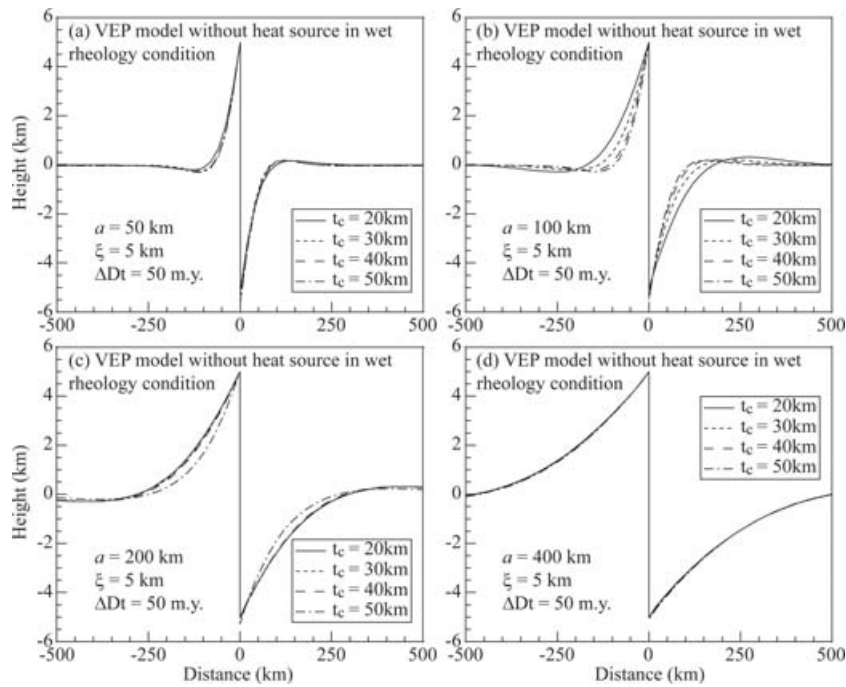
Figure 5. Surface deformation predicted by the viscoelastic–perfect plastic (VEP) model without heat source in wet rheology condition for different t_c; (a) $a = 50$ km, (b) $a = 100$ km, (c) $a = 200$ km and (d) $a = 400$ km.

4.1.3 *The half-wavelength of the flexural uplift in the VEP model with uniform lithosphere structure*

In Figs 6(a) and (b), we summarize the half-wavelength of the flexural uplift (λ) as a function of a for different t_c in the wet rheology condition, where $\xi = 5$ km and the duration of extension (ΔD_t) = 50 Myr. λ is generally greater for the model without a radiogenic heat source than for the model with a heat source. λ is also greater for the model with smaller t_c and greater a, regardless of the presence of a heat source. For the model with a heat source, λ has a
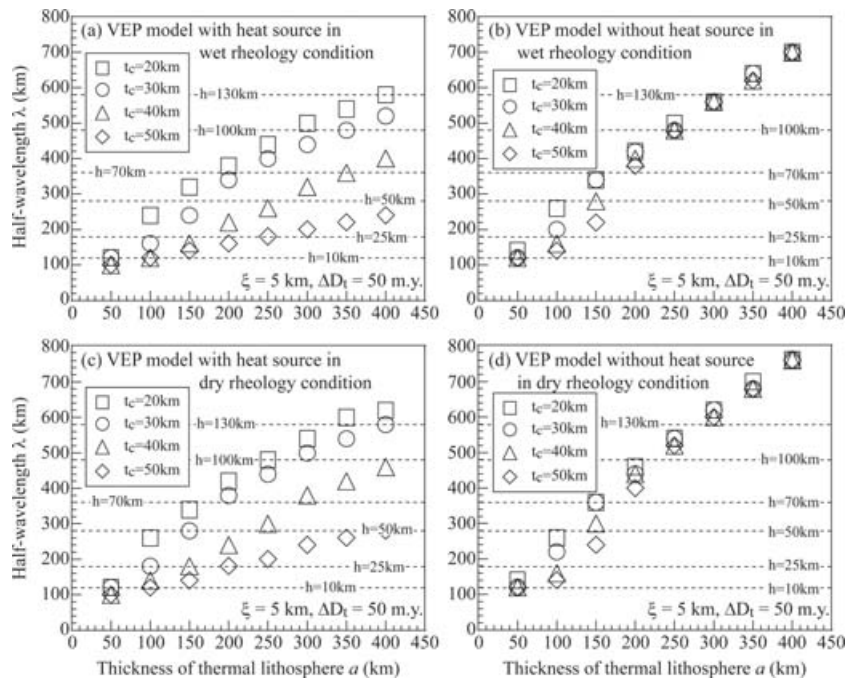

Figure 6. Predicted half-wavelength λ by the VEP model as a function of a for different t_c. The extensional period (ΔD_t) is 50 Myr, and the magnitude of the uplift at the mountain front (ξ) is 5 km. Predicted λ by the simple viscoelastic (VE) model as a function of the thickness of elastic layer (h) is depicted by horizontal dashed line. (a) Model with heat source in wet rheology condition, (b) model without heat source in wet rheology condition, (c) model with heat source in dry rheology condition and (d) model without heat source in dry rheology condition.

strong dependence on t_c when a is more than 100 km. In contrast, for the model without a heat source, λ is significantly dependent on t_c only when a is $100 \leq a \leq 200$ km.

λ in the dry rheology condition is summarized in Figs 6(c) and (d). λ is greater in the dry rheology condition than in the wet rheology condition. However, the lithospheric structure to obtain a particular λ is not widely different from that in the wet rheology condition.

The effective elastic thickness (T_e) is inferred from the comparison of λ in the VEP model with that in the simple viscoelastic (VE) model. Horizontal dashed lines show λ predicted by the VE model in which the elastic layer with a thickness of h overlays the viscoelastic layer with uniform viscosity η_m ($= 5 \times 10^{20}$ Pa s from Nakada *et al.* 2000). In this study, we have confirmed that λ is controlled only by h in the VE model. As can be seen in the figure, the lithosphere structure can be strictly constrained to obtain a certain value of T_e.

The dependence of λ on ξ in the wet rheology condition is shown in Fig. 7. Results for the models with $\xi = 10$ km are shown in Figs 7(a) and (b) and those for the models with $\xi = 2.5$ km in Figs 7(c) and (d). λ predicted by the VE model is also shown in the figures. ξ has an influence on λ; the model with smaller ξ predicts greater λ. However, the difference in λ between the models with $\xi = 2.5$ and 10 km is about 60 km at most, so that the lithospheric structure to obtain a particular λ is not changed largely. We have also confirmed the sensitivity of λ to the duration of extension ($\Delta D_t = 25$, 50 or 100 My) is insignificant.

4.2 Model results of the TAM

4.2.1 *The modelled temperature distribution beneath East and West Antarctica*

Fig. 8 shows the temperature distribution for the TM01 and TM02 models. Figs 8(a) and (b) are for the models with a radiogenic heat source in the crust and mantle, and Figs 8(c) and (d) are for the models without a heat source. In the TM01 model, the thickness of the thermal lithosphere is changing with distance in the model. The maximum thickness of the thermal lithosphere beneath East ($a_e = 250$ km) and West ($a_w = 90$ km) Antarctica are defined at distances of -1500 and 1500 km, respectively. On the other hand, in the TM02 model, each of East and West Antarctica has the thermal lithosphere with uniform thickness, a_e and a_w, respectively. Thus, the thermal structure beneath East Antarctica is significantly influenced by the heat flow from West Antarctica in the TM01 model but not at all in the TM02 model.

The geothermal gradient is significantly smaller for the model without a heat source than for the model with a heat source, especially at shallower depth in the lithosphere. However, it can be seen that for the TM01 model with a heat source, the geothermal gradient beneath the margin of East Antarctica is greater than that beneath the margin of West Antarctica. This is because the thickness of the crust beneath East Antarctica is greater than that beneath West Antarctica.

4.2.2 *The surface deflection without the load of the ice sheet*

Fig. 9 shows the surface deformation predicted by the VEP model without the load of the ice sheet. V_x is adjusted to obtain $\xi = 7.5$ km at $t = 50$ Myr. To estimate the effective elastic thickness (T_e) in the VEP model, the surface deformation predicted by the VE model is also depicted in the figures. For the TM01 model with a heat source (see Fig. 9a), the half-wavelength in East Antarctica (λ_e) is predicted to be 170 km, which is consistent with $T_e \sim 25$ km (see Figs 6 and 7). However, T_e beneath the edge of East Antarctica ($x = 0$–50 km) seems to be less than 10 km. It is likely that T_e increases as the depth of the isotherm increases, but the maximum T_e in the relevant region corresponds to that inferred from λ. On the
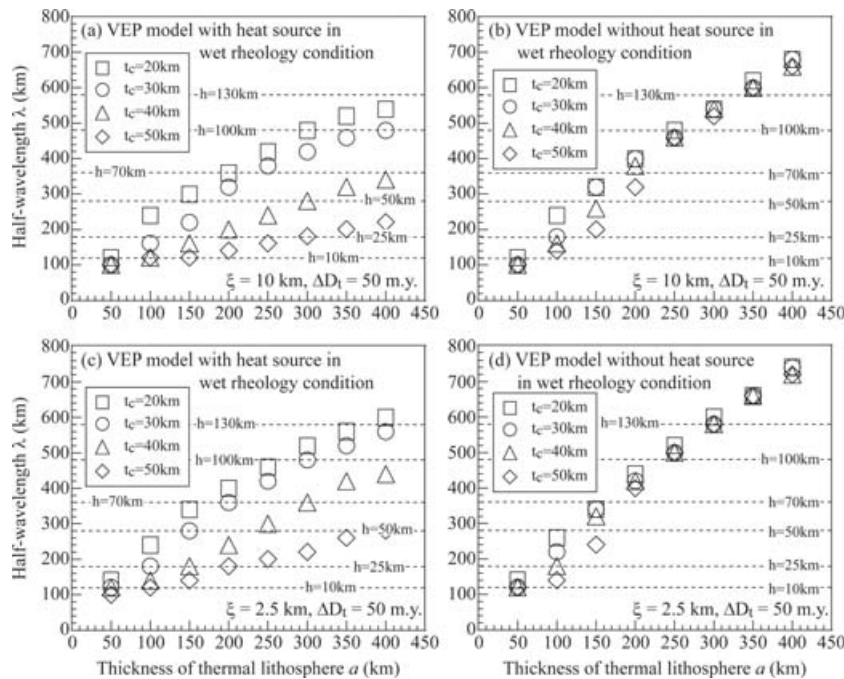

Figure 7. Predicted half-wavelength λ by the VEP model as a function of a for different t_c. ΔD_t is 50 Myr. Predicted λ by the VE model as a function of h is depicted by horizontal dashed line. (a) $\xi = 10$ km for the model with heat source in wet rheology condition, (b) $\xi = 10$ km for the model without heat source in wet rheology condition, (c) $\xi = 2.5$ km for the model with heat source in wet rheology condition and (d) $\xi = 2.5$ km for the model without heat source in wet rheology condition.
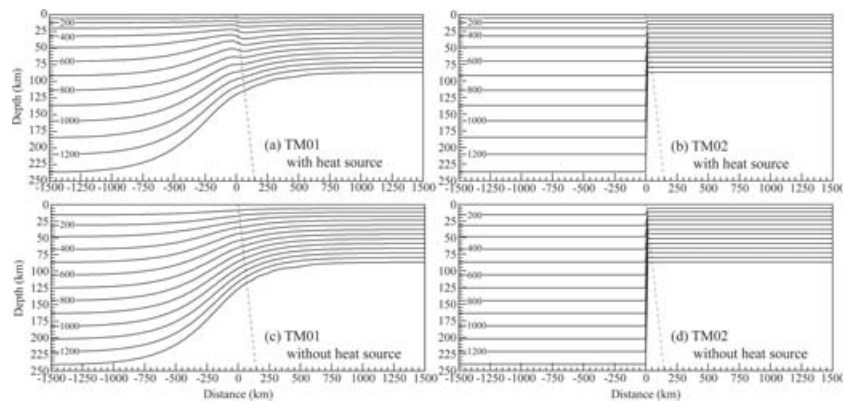
Figure 8. The temperature distribution beneath Antarctica adopted in this study. The location of the border fault is indicated by the dashed line. (a) TM01 model with heat source, (b) TM02 model with heat source, (c) TM01 model without heat source and (d) TM02 model without heat source.
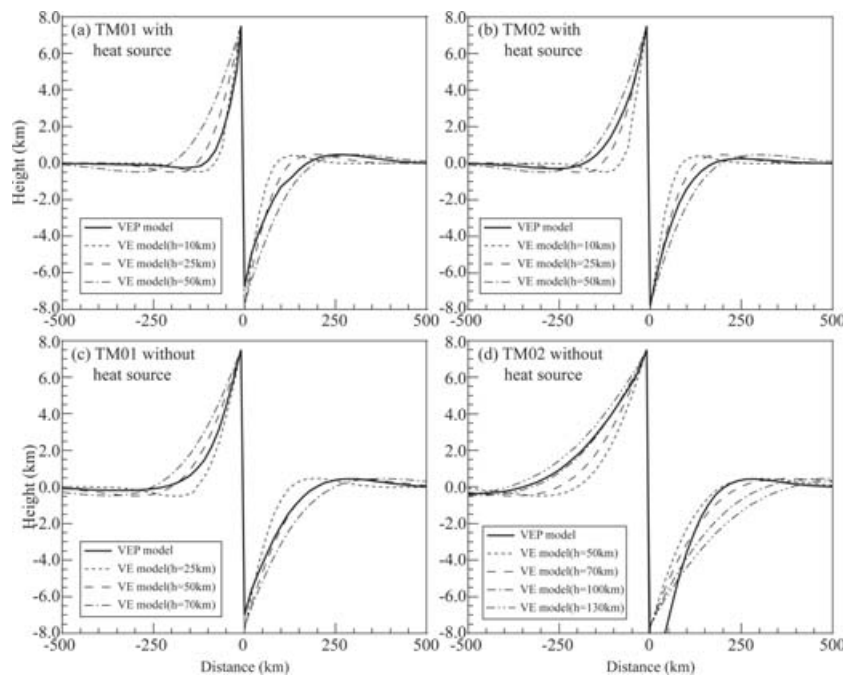

Figure 9. Surface deformation in East and West Antarctica predicted by the VEP and VE models without the load of the ice sheet. (a) TM01 model with heat source, (b) TM02 model with heat source, (c) TM01 model without heat source and (d) TM02 model without heat source.

other hand, for the TM02 model with a heat source (see Fig. 9b), T_e beneath East Antarctica is between 25 and 50 km. λ_e is 270 km, from which T_e is estimated to be just slightly less than 50 km (see Figs 6 and 7).

For the TM01 model without a heat source (see Fig. 9(c)), T_e beneath East Antarctica seems significantly less than 50 km beneath the margin of the East Antarctica, but the 320 km of λ_e indicates that T_e is about 60 km (see Figs 6 and 7). This also implies the regional difference in T_e, depending on the thermal structure beneath East Antarctica. On the other hand, for the TM02 model without a heat source (see Fig. 9d), the surface deformation mostly matches with that predicted by the VE model with $h = 100$ km, and λ_e is predicted to be about 500 km.

The half-wavelengths in West Antarctica (λ_w) for the TM01 and TM02 models with a heat source are 250 and 200 km, respectively, and T_e beneath West Antarctica is estimated to be between 25 and 50 km for the both models (see Figs 9a and b). λ_w is slightly larger

for the TM01 model than for the TM02 model. This is because the temperature beneath the edge of West Antarctica is reduced by the lateral heat flow to East Antarctica in the TM01 model. On the other hand, for the models without a heat source, λ_w is about 250 km, which is equivalent to $T_e \sim 50$ km (see Figs 9c and d).

4.2.3 The stress distribution in the lithosphere without the load of the ice sheet

Fig. 10 shows the distribution of the stress σ_{xx} in the lithosphere beneath East Antarctica, for the model without the load of the ice sheet. For the TM01 model with a heat source, the brittle–ductile transition can be seen at the depth of 5 km at all distances (see Fig. 10a). Any competent elastic cores cannot be seen at the distances of −50 and −300 km. However, at the distances of −500 and −1490 km, the elastic cores are present in the uppermost mantle. It is noted that the estimated T_e is slightly greater than the
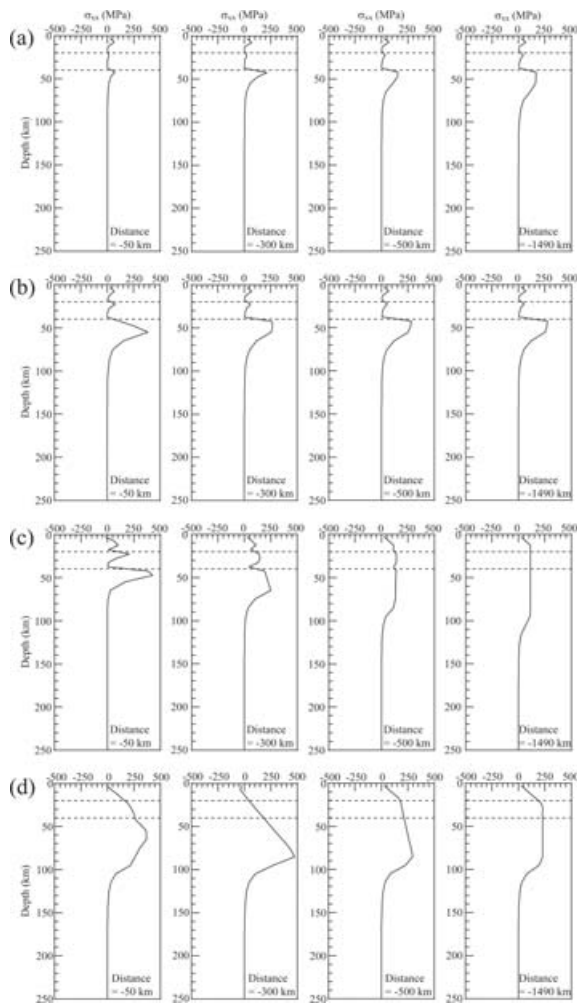
Figure 10. Distribution of the stress σ_{xx} in the lithosphere beneath East Antarctica for the model without the load of the ice sheet. Horizontal dashed lines indicate the boundary between the upper crust and lower crust and the Moho. (a) TM01 model with heat source, (b) TM02 model with heat source, (c) TM01 model without heat source and (d) TM02 model without heat source.

seismogenic thickness in the upper crust, as indicated by Watts & Burov (2003).

For the TM02 model with a heat source (Fig. 10b), the competent elastic core can be seen at a depth between 40 and 55 km at all distances. The bottom of the estimated effective elastic layer seems to be located in the elastic core just below the Moho.

For the TM01 model without a heat source (Fig. 10c), the presence of the mechanically competent layer is dependent on the distance from the mountain front, as was seen in the TM01 model with a heat source (Fig. 10a). This is consistent with the thermal structure of the TM01 model depicted in Figs 8(a) and (c), in which the depth of the isotherm increases as the distance from West Antarctica increases. The competent elastic cores are present at depths between 40 and 45 km and between 40 and 65 km at distances -50 and -300 km, respectively. The bottom of the estimated effective elastic layer is located in the elastic core at each distance. Additionally, the stress distribution at a distance less than -500 km shows that the elastic core is extended to the depth of 95 km, at most.

For the TM02 model without a heat source (Fig. 10d), the mechanically competent layer is extended to a depth of $\sim$95 km at all distances, so that the estimated T_e ($\sim$100 km) is mostly equivalent to the extent depth of the elastic core.

4.2.4 The surface deflection with the load of the ice sheet

Figs 11(a) and (b) show the surface deformations predicted by the TM01 and TM02 models, respectively, with the load of the ice sheet, where a radiogenic heat source is present in the crust and mantle. For comparison, the surface deformation predicted by the model without the load of the ice sheet is also depicted in the figures. Shaded bands indicate the observed ranges of λ_e and λ_w. When the IM01 model is adopted for the load of the ice sheet, λ_e is predicted to be 350 and 300 km by the TM01 and TM02 model, respectively. However, when the IM02 model is adopted for the load of the ice sheet, the half-wavelength of the TAM can be reproduced even by the TM01 model in which the topographic minimum point in East Antarctica is located at a distance of $\sim$$-500$ km. It is difficult for the TM02 model to predict the topographic minimum point in the East Antarctica.

Although λ_e is greater for the model with the load of the ice sheet than for the model without the load of the ice sheet, λ_w is not affected by the load of the ice sheet at all. However, the predicted λ_w is consistent with the observation for both the TM01 and TM02 models.

Figs 11(c) and (d) show the surface deformations predicted by the TM01 and TM02 models, respectively, without a radiogenic heat source. When the TM01 is adopted for the thermal structure beneath Antarctica, λ_e is predicted to be 380 km for the IM01 model, and it is difficult to reproduce the half-wavelength of the TAM. However, λ_e is predicted to be 520 km for the IM02 model, which is consistent with that of the TAM. On the other hand, when the TM02 model is adopted for the thermal structure, λ_e is predicted to be 500 and 540 km for the IM01 and IM02 models, respectively. The model behaviour of the surface deflection in West Antarctica is similar to that for the model with a heat source, except that λ_w is slightly larger than 250 km.

5 DISCUSSION

5.1 Factors controlling the effective elastic thickness (T_e)

As in earlier models, we show that the effective elastic thickness (T_e) inferred from the half-wavelength of the flexural uplift (λ) is greater for the model with smaller thickness of the crust (t_c) and greater thickness of the thermal lithosphere (a) (e.g. Watts 1978; Watts *et al.* 1980; McNutt & Menard 1982; McAdoo *et al.* 1985; Burov & Diament 1995). Radiogenic heat production increases with decreasing lithospheric age (e.g. Turcotte & Schubert 1982), and it also becomes an important factor controlling flexural rigidity in Antarctica through the temperature-dependent viscosity (e.g. Pérez-Gussinyé & Watts 2005).

It is also shown that λ is slightly dependent on the magnitude of the uplift (ξ) in the VEP model (see Fig. 7). This may imply that T_e is also sensitive to deformation-induced stresses, as pointed out by Burov & Diament (1995), because rheological properties are strongly controlled by stress state in the VEP model. In this regard, the observed ξ should be accurately constrained as much as possible when T_e is estimated from λ. However, the lithospheric structure to obtain a particular λ is not largely influenced by ξ (see Figs 6 and 7).
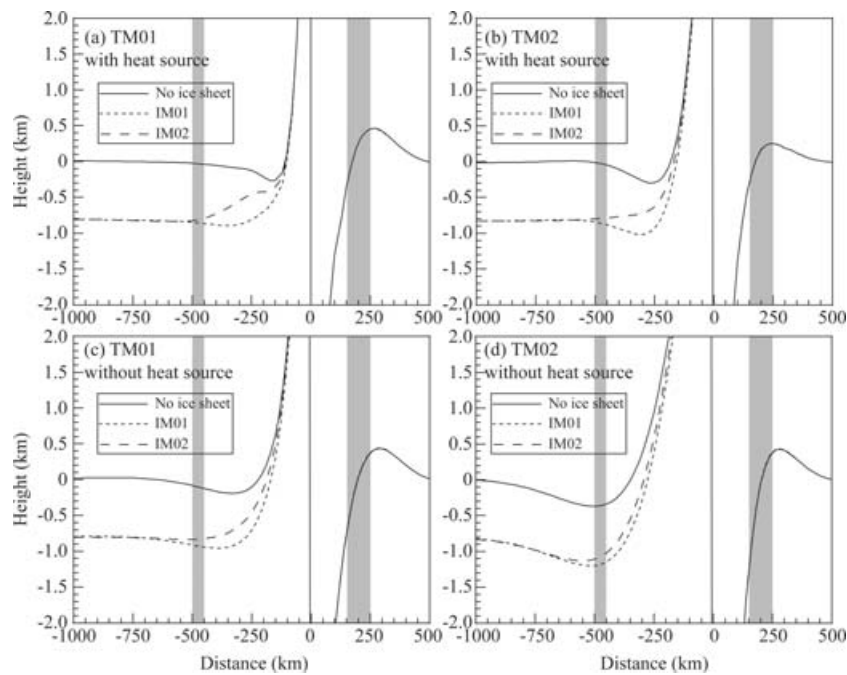
Figure 11. Surface deformation in East and West Antarctica predicted by the VEP model for different ice sheet models. (a) TM01 model with heat source, (b) TM02 model with heat source, (c) TM01 model without heat source and (d) TM02 model without heat source.

5.2 Insights into the half-wavelength of the TAM

5.2.1 The case where a radiogenic heat source is present in the Antarctic lithosphere

The thermal structure beneath Antarctica is the critical factor controlling the half-wavelength of the flexural uplift in East Antarctica (λ_e). When a heat source is present, λ_e and T_e are predicted to be 170–270 km and 25–50 km, respectively, at most, by the model without the load of the ice sheet, depending on the thermal state beneath the margin of East Antarctica. Therefore, the rheological structure beneath East Antarctica has no potential to produce the half-wavelength of the TAM if a significant heat source is present in the crust and mantle. Heat flow from West Antarctica reduces the thickness of the thermal lithosphere beneath the margin of East Antarctica, which further prevents the half-wavelength of the TAM being obtained (see the TM01 model in Figs 8 and 9). Even when the thickness of the crust beneath East Antarctica (t_{ce}) is assumed to be 35 km (Lawrence *et al.* 2006), the half-wavelength of the TAM is still difficult to explain (see Figs 6 and 7). It is also difficult to reproduce the half-wavelength of the TAM even in a dry rheology condition (see Fig. 6). Additionally, the uncertainties in the estimated magnitude of rock uplift and lithosphere thickness seem impossible to explain the half-wavelength of the TAM (see Figs 6 and 7).

Although the unloading due to surface erosion is not taken into account in the numerical model of this study, Burov & Diament (1995) indicated that the effect of erosion can possibly increase T_e (∼20 per cent). However, it is questionable if the 20 per cent increase in T_e due to the erosion is enough to influence the estimate of the half-wavelength of the TAM. Additionally, significant erosion has taken place only to the distances of ∼150 km from the TAM's front (e.g. ten Brink *et al.* 1997). Even if a significant increase in T_e could be brought about by the erosion, only a locally increased T_e may be still difficult to explain the half-wavelength of the TAM.

λ_e can be predicted to be only the typical scale of the rift flank uplift observed in many rift systems, but much less than that of the TAM, when a radiogenic heat source is present in the crust and mantle. The half-wavelength of the TAM may have to be explained by the locally compensated ice load. ten Brink *et al.* (1997) pointed out that the load of the ice sheet can widen the apparent half-wavelength of flexure. However, as shown in Fig. 11, the IM01 model of the ice sheet that is the same as ten Brink *et al.* (1997), cannot reproduce the half-wavelength of the TAM. The most that can be done at the moment is, therefore, to adjust the external load of the ice sheet. To reproduce the half-wavelength of the TAM, we construct the IM02 model of the ice sheet in this study, in which the maximum thickness of the ice sheet is attained at the point where the axis of the Wilkes Basin is located (see Fig. 2). This assumption may be reasonable because the height of the ice sheet surface seems mostly constant though the subglacial topographic height decreases towards the deepest point of the Wilkes Basin (see the profiles along the EAST93 traverse in ten Brink *et al.* 1997). In addition, the sediment load in the hinterland may also help to widen the half-wavelength of flexure (ten Brink & Stern 1992).

However, there is a serious problem with the model including a radiogenic heat source. Since local isostatic compensation of the large-scale ice sheet and/or sediment load would have been mostly completed, there would be no significant gravity anomaly. Additionally, the distinct surface depression corresponding to the Wilkes Basin is difficult to obtain in our model with a heat source. The distinct surface depression behind the TAM may have to be explained by a locally thickened ice sheet. Nevertheless, a locally thickened ice sheet is unlikely to develop without a pre-existing depression. Furthermore, even though Stern & ten Brink (1989) correlated the Wilkes Basin with the TAM's uplift in terms of flexure model, the rheological structure beneath East Antarctica has no potential to create the surface depression there. Thus, if a significant amount of heating lies within the Antarctic lithosphere, we conclude that the surface depression corresponding to the Wilkes Basin had no

relation to the uplift of the TAM, and further work is obviously required to elucidate the mechanism to explain its origin.

5.2.2 The case where a radiogenic heat source is not present in the Antarctic lithosphere

When a radiogenic heat source is not present in the crust and mantle, it is possible for the TM02 model to obtain $\lambda_e \sim 500$ km ($T_e \sim 100$ km) in which East Antarctica is not thermally influenced by West Antarctica at all. On the other hand, if the thermal structure beneath East Antarctica is significantly influenced by the lateral heat flow from West Antarctica (in the TM01 model), T_e is estimated to be about 60 km at most and the half-wavelength of the TAM is difficult to reproduce without including the effect of the load of the ice sheet. Stern & ten Brink (1989), Bott & Stern (1992) and ten Brink & Stern (1992) indicated that a 100 km thick elastic layer is essentially required to produce the half-wavelength of the TAM. Based on new geophysical data ten Brink *et al.* (1997) re-evaluated the required elastic thickness to be 85 ± 15 km. Such a thickness of the effective elastic layer ($T_e \sim 100$ km) is available for the VEP model with a plausible lithospheric structure beneath Antarctica only when a radiogenic heat source is absent and the thermal structure beneath East Antarctica is not significantly affected by that beneath West Antarctica. The relatively thin elastic layer beneath the mountain front (5–25 km) evaluated in these prior studies may correspond to the thermal influence from West Antarctica on the margin of East Antarctica. However, such a thermal influence must be limited only to the edge of East Antarctica to obtain the large-scale half-wavelength of the TAM.

6 CONCLUSIONS

This study has discussed the uplift of the TAM in relation to the flexural uplift of the rheologically layered lithosphere in Vening-Meinesz's cantilever kinematics. We have examined first the general model behaviour in the VEP rheology model with temperature dependence of viscosity. We then applied the VEP model to the uplift of the TAM, respecting the lithospheric structure beneath Antarctica inferred from geophysical observations and the load of the ice sheet in East Antarctica. This study gives important insights into the uplift of the TAM, especially its half-wavelength, in relation to the rheological structure beneath Antarctica. The conclusions are as follows:

(1) The thicknesses of the crust (t_c) and thermal lithosphere (a) are the principal factors controlling the effective elastic thickness (T_e) inferred from the half-wavelength of the flexural uplift; the model with smaller t_c and greater a results in greater T_e. The model without a heat source also results in greater T_e than the model with a heat source. It is found that t_c must be taken into account in the estimate of T_e under the following conditions of the thermal lithosphere; $a \geq 100$ km for the model with a heat source and $100 \leq a \leq 200$ km for the model without a heat source. T_e is also significantly dependent on the magnitude of the uplift and the wet or dry rheology condition of rocks, but these factors are not able to conclusively control the uplift of the TAM.

(2) The presence of a radiogenic heat source in the Antarctic lithosphere and the thermal influence of West Antarctica on East Antarctica are the critical factors in controlling the half-wavelength of the TAM. When a heat source is present, the rheological structure beneath East Antarctica ($T_e = 25$–50 km) has no potential to reproduce the half-wavelength of the TAM. To explain the distance from the TAM front to the axis of the Wilkes Basin, it is necessary to fall back upon the load of the ice sheet. On the other hand, when a heat source is absent and the thermal structure beneath East Antarctica is not significantly affected by that beneath West Antarctica, it is possible for the rheological structure beneath East Antarctica ($T_e \sim 100$ km) to reproduce the half-wavelength of the TAM. However, if the thermal structure beneath East Antarctica is significantly influenced by West Antarctica, T_e is predicted to be about 60 km, and it is therefore difficult, even for the model without a heat source, to reproduce the half-wavelength of the TAM without considering the load of the ice sheet.

REFERENCES

Artemjev, M.E. & Artyushkov, E.V., 1971. Structure and isostasy of the Baikal Rift and the mechanism of rifting, *J. geophys. Res.*, **76,** 1197–1211.

Bannister, S., Yu, J., Leitner, B. & Kennett, B.L., 2003. Variations in crustal structure across the transition from West to East Antarctica, Southern Victoria Land, *Geophys. J. Int.,* **155,** 870–844.

Barker, P.F., Barrett, P.J. Cooper, A.K. & Huybrechts, P., 1999. Antarctic glacial history from numerical models and continental margin sediments, *Palaeogeogr. Palaeoclimatol. Palaeoecol.*, **150,** 247–167.

Barrett, P.J., Hambrey, M.J., Harwood, D.M., Pyne, A.R. & Webb P.-N., 1989. Synthesis—Antarctic Cenozoic history from the CIROS-1 drill hole, McMurdo Sound, *N.Z. Dep. Sci. Ind. Res. Bull.,* **245,** 241–251.

Bassi, G., 1991. Factors controlling the style of continental rifting: insights from numerical modelling, *Earth planet. Sci. Lett.*, **105,** 430–452.

Bassi, G., 1995. Relative importance of strain rate and rheology for the mode of continental extension, *Geophys. J. Int.,* **122,** 195–210.

Bentley, C.R., 1983. Crustal structure of Antarctica from geophysical evidence—a review, in *Proceedings of the Fourth International Symposium on Antarctic Earth Sciences*, pp. 491–497, eds Oliver, R.L., James, P.R. & Jago, J.B., Cambridge University Press, New York.

Berg, J.H., Moscati, R.J. & Herz, D.L., 1989. A petrologic geotherm from a continental rift in Antarctica, *Earth planet. Sci. Lett.,* **93,** 98–108.

Bialas, R.W., Buck, W.R., Studinger, M. & Fitzgerald, P.G., 2007. Plateau collapse model for the Transantarctic Mountains – West Antarctic Rift System: insights from numerical experiments, *Geology,* **35,** 687–690.

Blackman, D.K., Von Herzen, R.P. & Lawver, L.A., 1987. Heat flow and tectonics in the western Ross Sea, Antarctica, in *The Antarctic Continental Margin: Geology and Geophysics of the Western Ross Sea,* **Vol. 5B**: Earth Science Series, pp. 179–189, eds Cooper, A.K. & Davey, F.J., Circum-Pacific Council for Energy and Natural Resources, Houston, Texas.

Bonini, M., Corti, G., Del Ventisette, C., Manetti, P., Mulugeta, G. & Sokoutis D., 2007. Modelling the lithosphere rheology control on the Cretaceous rifting in West Antarctica, *Terra Nova,* **19,** 360–366.

Bott, M.H.P. & Stern, T.A., 1992. Finite element analysis of Transantarctic Mountain uplift and coeval subsidence in the Ross Embayment, *Tectonophysics,* **201,** 341–356.

Brace, W.F. & Kohlstedt, D.L., 1980. Limits on lithospheric stress imposed by laboratory experiments, *J. geophys. Res.,* **85,** 6248–6252.

Braun, J., 1988. Styles of continental extension: results from numerical experiments, *PhD thesis.* pp. 352, Dalhousie University, Halifax, Nova Scotia.

Braun, J. & Beaumont, C., 1987. Styles of continental rifting: results from dynamic models of lithospheric extension, in *Sedimentary Basins and Basin Forming Mechanisms,* Memoir **12,** pp. 241–258, eds Beaumont, C. & Tankard, A.J., *Can. Soc. Petrol. Geol*.

Braun, J. & Beaumont, C., 1989. A physical explanation of the relation between flank uplifts and breakup unconformity at rifted continental margins, *Geology,* **17,** 760–764.

Burov, E.B. & Diament, M., 1992. Flexure of the continental lithosphere with multilayered rheology, *Geophys. J. Int.,* **109,** 449–468.

Burov, E.B. & Diament, M., 1995. The effective elastic thickness (T_e) of continental lithosphere: what does it mean? *J. geophys. Res.,* **100,** 3905–3927.

Byerlee, J.D., 1967. Frictional characteristics of granite under high confining pressure, *J. geophys. Res.,* **72,** 3639–3648.

Byerlee, J.D., 1978. Friction of rocks, *Pure appl. Geophys.,* **116,** 615–626.

Carter, N.L. & Tsenn, M.C., 1987. Flow properties of continental lithosphere, *Tectonophysics,* **136,** 27–63.

Chopra, P.N. & Paterson, M.S., 1984. The role of water in the deformation of dunite, *J. geophys. Res.,* **89,** 7861–7876.

Cooper, A.K., Davey, F.J. & Behrendt, J.C., 1991a. Structural and depositional controls on Cenozoic and (?) Mesozoic strata beneath the western Ross Sea, in *Geological Evolution of Antarctica,* pp. 279–283, eds Thomson, M.R.A., Crame, J.A. and Thomson, J.W., Cambridge University Pres, New York.

Cooper, A.K., Davey, F.J. & Hinz, K., 1991b. Crustal extension and origin of sedimentary basins beneath the Ross Sea and Ross Ice Shelf, Antarctica, in *Geological Evolution of Antarctica,* pp. 285–291, eds Thomson, M.R.A., Crame, J.A. & Thomson, J.W., Cambridge University Pres, New York.

Danesi, S. & Morelli, A., 2000. Group velocity of Rayleigh waves in the Antarctic region, *Phys. Earth planet. Inter.,* **122,** 55–66.

Danesi, S. & Morelli, A., 2001. Structure of the upper mantle under the Antarctic plate from surface wave tomography, *Geophys. Res. Lett.,* **28,** 4395–4398.

Della Vedova, B., Pellis, G., Lawver, L.A. & Brancolini, G., 1992. Heat flow and tectonics of the Western Ross Sea, in *Recent Progress in Antarctic Earth Science,* pp. 627–637, eds, Yoshida, Y., Kaminuma, K. & Shiraishi, K., Terrapub, Tokyo.

Drewry, D.J., 1976. Sedimentary basins of the east Antarctic craton from geophysical evidence, *Tectonophysics,* **36,** 301–314.

Drewry, D.J., 1983. *Antarctica: Glaciological and Geophysical Folio,* Scott. Polar Res. Inst., Cambridge.

Ebinger, C.J., Karner, G.D. & Weissel, J.K., 1991. Mechanical strength of extended continental lithosphere: constraints from the Western rift system, Africa, *Tectonics,* **10,** 1239–1256.

England, P.C. & Molnar, P., 1990. Surface uplift, uplift of rocks and exhumation of rocks, *Geology,* **18,** 1173–1177.

Fitzgerald, P.G., 1992. The Transantarctic Mountains of Southern Victoria Land: the application of apatite fission track analysis to a rift shoulder uplift, *Tectonics,* **11,** 634–662.

Fitzgerald, P.G., 1994. Thermochronologic constraints on post-Paleozoic tectonic evolution of the central Transantarctic Mountains, Antarctica, *Tectonics,* **13,** 818–836.

Fitzgerald, P.G., Sandiford, M., Barrett, P.J. & Gleadow, A.J.W., 1986. Asymmetric extension associated with uplift and subsidence in the Transantarctic Mountains and Ross Embayment, *Earth planet. Sci. Lett.,* **81,** 67–78.

Fletcher, R.C. & Hallet, B., 1983. Unstable extension of the lithosphere: a mechanical model for Basin and Range structure, *J. geophys. Res.,* **88,** 7457–7466.

Goetze, C. & Evans, B., 1979. Stress and temperature in the bending lithosphere as constrained by experimental rock mechanics, *Geophys. J. R. astr. Soc.,* **59,** 463–478.

Govers, R. & Wortel, M.J.R., 1993. Initiation of asymmetric extension in continental lithosphere. *Tectonophysics,* **223,** 75–96.

Govers, R. & Wortel, M.J.R., 1995. Extension of stable continental lithosphere and the initiation of lithospheric scale faults, *Tectonics,* **14,** 1041–1055.

Huerta, A.D. & Harry, D.L., 2007. The transition from diffuse to focused extension: model evolution of the West Antarctic Rift system, *Earth planet. Sci. Lett.,* **225,** 133–147.

Huismans, R.S. & Beaumont, C., 2002. Asymmetric lithospheric extension: the role of frictional plastic strain softening inferred from numerical experiments, *Geology,* **30,** 211–214.

Kirby, S.H., 1983. Rheology of the lithosphere, *Rev. Geophys. Space Phys.,* **21,** 1458–1487.

Koch, P.S., Christie, J.M., Ord, A. & George R.P., Jr, 1989. Effect of water on the rheology of experimentally deformed quartzite, *J. geophys. Res.,* **94,** 13 975–13 996.

Kohlstedt, D.L., Evans, B. & Mackwell, S.J., 1995. Strength of the lithosphere: constraints imposed by laboratory experiments, *J. geophys. Res.,* **100,** 17 587–17 602.

Kooi, H., Cloetingh, S. & Burrus, J., 1992. Lithospheric necking and regional isostasy at extensional basins 1. Subsidence and gravity modeling with an application to the Gulf of Lions margin (SE France), *J. geophys. Res.,* **97,** 17 553–17 571.

Krieg, R.D. & Krieg, D.B., 1977. Accuracies of numerical solution methods for the elastic-perfectly plastic model, *Tans. ASME, J. Pressure Vessel Tech.,* **99,** 510–515.

Lawrence, J.F., Wiens, D.A., Nyblade, A.A., Anandakrishnan, S., Shore, P.J. & Voigt, D., 2006. Crust and upper mantle structure of the Transantarctic Mountains and surrounding regions from receiver functions, surface waves, and gravity: implications for uplift models, *Geochem. Geophys. Geosys.,* **7,** doi:10.1029/2006GC001282.

McAdoo, D.C., Martin, C.F. & Polouse, S., 1985. Seasat observations of flexure: evidence for a strong lithosphere, *Tectonophysics,* **116,** 209–222.

McNutt, M. & Menard, H.W., 1982. Constraints on the yield strength in the oceanic lithosphere derived from observations of flexure, *Geophys. J. R. astr. Soc.,* **59,** 4663–4678.

Melosh, H.J. & Raefsky, A., 1980. The dynamical origin of subduction zone topography, *Geophys. J. R. astr. Soc.,* **60,** 333–354.

Melosh, H.J. & Raefsky, A., 1981. A simple and efficient method for introducing faults into finite element computations, *Bull. seism. Soc. Am.,* **71,** 1391–1400.

Melosh, H.J. & Williams, C.A., 1989. Mechanics of graben formation in crustal rocks: a finite element analysis, *J. geophys. Res.,* **94,** 13 961–13 973.

Miller, K.G., Fairbanks, R.G. & Mountain, G.S., 1987. Tertiary oxygen isotope synthesis, sea level history, and continental margin erosion, *Paleoceanography,* **2,** 1–19.

Nakada, M., Kimura, R., Okuno, J., Moriwaki, K., Miura, H. & Maemoku, H., 2000. Late Pleistocene and Holocene melting history of the Antarctic ice sheet derived from sea-level variations, *Mar. Geol.,* **167,** 84–103.

Pascal, C., van Wijk, J.W., Cloeting, S.A.P.L. & Davies, G.R., 2002. Effect of lithosphere thickness heterogeneities in controlling rift localization: numerical modeling of the Oslo Graben, *Geophys. Res. Lett.,* **29**(9), doi:10.1029/2001GL014354.

Pascal, C., Cloetingh, S.A.P.L. & Davies, G.R., 2004. Asymmetric lithosphere as the cause of rifting and magmatism in the Permo-Carboniferous Oslo Graben, in *Permo-Carboniferous Magmatism and Rifting in Europe,* Vol. **223,** pp. 139–156, eds Wilson, M., Neumann, E.-R.,Davies, G.R., Timmerman M.J. & Larsen, B.T., *Geol. Soc. Spec. Publ.,* London.

Petit, C. & Ebinger, C., 2000. Flexure and mechanical behavior of cratonic lithosphere: gravity models of the East African and Baikal rifts, *J. geophys. Res.,* **105,** 19 151–19 162.

Pérez-Gussinyé, M. & Watts, A.B., 2005. The long-term strength of Europe and its implications for plate-forming processes, *Nature,* **436,** 381–384, doi:10.1038/nature03854.

Ranalli, G., 1995. *Rheology of the Earth,* 2nd edn, pp. 413, Chapman and Hall, London.

Ranalli, G. & Murphy, D.C., 1987. Rheological stratification of the lithosphere, *Tectonophysics,* **132,** 281–295.

Robinson, E.S. & Splettstoesser, J.F., 1984. Structure of the Transantarctic Mountains determined from geophysical surveys, in *Geology of the Central Transantarctic Mountains,* Vol. **36:** Antarct. Res. Ser., pp. 119–162, eds Turner, M.D. & Splettstoesser, J.F., AGU, Washington, DC.

Shelton, G. & Tullis, J., 1981. Experimental flow laws for crustal rocks, *EOS, Trans. Am. geophys. Un.,* **62,** 396.

Sibson, R.H., 1977. Fault rocks and fault mechanisms, *J geol. Soc. Lond.,* **133,** 191–213.

Sieminski, A., Debayle, E. & Lévêque, J.-J., 2003. Seismic evidence for deep low-velocity anomalies in the transition zone beneath West Antarctica, *Earth planet. Sci. Lett.,* **216,** 645–661.

Steckler, S. M., 1985. Uplift and extension at the Gulf of Suez: indications of induced mantle convection, *Nature,* **317,** 135–139.

Steed, R.H.N., 1983. Structural interpretation of Wilkes Land, Antarctica, in *Proceedings of the Fourth International Symposiumon Antarctic Earth Sciences,* pp. 567–572, eds Oliver, R.L., James, P.R. & Jago, J.B., Cambridge University Press, New York.

Stern, T.A. & ten Brink, U.S., 1989. Flexural uplift of the transantarctic mountains, *J. geophys. Res.,* **94,** 10 315–10 330.

ten Brink, U. & Stern T., 1992. Rift flank uplifts and hinterland basins: comparison of the Transantarctic Mountains with the great escarpment of southern Africa, *J. geophys. Res.,* **97,** 569–585.

ten Brink, U.S., Bannister, S., Beaudoin, B.C. & Stern, T.A., 1993. Geophysical investigations of the tectonic boundary between East and West Antarctica, *Science,* **261,** 45–50.

ten Brink, U.S., Hackney, R.I., Bannister, S., Stern, T.A. & Makovsky, Y., 1997. Uplift of the Transantarctic Mountains and the bedrock beneath the East Antarctic ice sheet, *J. geophys. Res.,* **102,** 27 603–26 621.

Turcotte, D.L. & Schubert, G., 1982. *Geodynamics: Applications of Continuum Physics to Geological Problems,* John Wiley & Sons, New York, 450 pp.

Van Der Beek, P., 1997. Flank uplift and topography at the central Baikal Rift (SE Siberia): a test of kinematic models for continental extension, *Tectonics,* **16,** 122–136.

Van Der Beek, P., Cloetingh, S. & Andriessen, P., 1994. Mechanisms of extensional basin formation and vertical motions at rift flanks: constraints from tectonic modelling and fission-track thermochronology, *Earth planet. Sci. Lett.,* **121,** 417–433.

Vening-Meinesz, F.A., 1950. Les Graben Africains, resultat de compression ou de tension dans la croûte terrestre? *Bull. Inst. R. Col. Belge,* **21,** 539–552.

Watts, A.B., 1978. An analysis of isostasy in the world's oceans, 1, Hawaiian-Emperor Seamount Chain, *J. geophys. Res.,* **83,** 5989–6004.

Watts, A.B. & Burov, E.B., 2003. Lithospheric strength and its relationship to the elastic and seismogenic layer thickness, *Earth planet. Sci. Lett.,* **213,** 113–131.

Watts, A.B., Bodine, J.H. & Ribe, N.M., 1980. Observations of flexure and geological evolution of the Pacific Ocean basin, *Nature,* **283,** 532–537.

Weissel, J.K. & Karner, G.D., 1989. Flexural uplift of rift flanks due to numerical unloading of the lithosphere during extension, *J. geophys. Res.,* **94,** 13 919–13 950.

Williams, C.A. & Richardson, R.M., 1991. A rheologically layered three-dimensional model of the San Andreas fault in central and southern California, *J. geophys. Res.,* **96,** 16 597–16 623.

Woodruff, F., Savin, S.M. & Douglas, R.G., 1981. Miocene stable isotope record: a detailed deep Pacific Ocean study and its paleoclimatic implications, *Science,* **212,** 665–668.

Zachos, J.C., Breza, J., Wise, S., Kennett, J., Stott, L. & the ODP Leg 120 Shipboard Scientific Party, 1989. A high latitude, southern Indian Ocean, Middle Eocene to Oligocene paleoclimatic record, *EOS, Trans Am. geophys. Un.,* **70,** 375.

Zachos, J., Pagani, M., Sloan, L., Thomas, E. & Billups, K., 2001. Trends, rhythms, and aberrations in global climate 65 Ma to present, *Science,* **292,** 686–693.